4. Miyashita, N. T. *Genetics* **125,** 407 419 (1990).
5. Miyashita, N. & Langley, C. H. *Genetics* **120,** 199 212 (1988).
6. Martin-Campos, J. M., Cameron, J. M., Miyashita, N. & Aguadé, M. *Genetics* **130,** 805 816 (1992).
7. Langley, C. H., MacDonald, J., Miyashita, N. & Aguadé, M. *Proc. natn. Acad. Sci. U.S.A.* **90,** 1800 1803 (1993).
8. Hudson, R. R., Boos, D. D. & Kaplan, N. L. *Molec. Biol. Evol.* **9,** 138-151 (1992).
9. Tajima, F. *Genetics* **123,** 585 595 (1989).
10. Eanes, W. F., Ajioka, J. W., Hey, J. & Wesley, C. *Molec. Biol. Evol.* **6,** 384-397 (1989).
11. Eanes, W. F., Labate, J. & Ajioka, J. W. *Molec. Biol. Evol.* **6,** 492 502 (1989).
12. Singh, R. S., Hickey, D. L. & David, J. *Genetics* **101,** 235-256 (1982).
13. David, J. R. & Capy, P. *Trends Genet.* **4,** 106-111 (1988).
14. Begun, D. J. & Aquadro, C. F. *Nature* **356,** 519-520 (1992).
15. Maynard Smith, J. & Haigh, J. *Genet. Res.* **23,** 23-35 (1974).
16. Kaplan, N. L., Hudson, R. R. & Langley, C. H. *Genetics* **123,** 887-899 (1989).
17. Charlesworth, B., Morgan, M. T. & Charlesworth, D. *Genetics* **134,** 1289-1303 (1993).
18. Stephan, W. & Mitchell, S. J. *Genetics* **132,** 1039-1045 (1992).
19. Hudson, R. *Oxf. Surv. evol. Biol.* **7,** 1-44 (1990).
20. Kreitman, M. & Aguadé, M. *Proc. natn. Acad. Sci. U.S.A.* **83,** 3562-3566 (1986).
21. Hudson, R. R. *Genetics* **100,** 711 719 (1982).
22. Nei, M. & Li, W.-H. *Proc. natn. Acad. Sci. U.S.A.* **76,** 5269-5273 (1979).
23. Hudson, R. R., Slatkin, M. & Maddison, W. P. *Genetics* **132,** 583-589 (1992).
24. Hudson, R. R., Kreitman, M. & Aguadé, M. *Genetics* **116,** 153-159 (1987).
25. Kreitman, M. & Hudson, R. R. *Genetics* **127,** 565-582 (1991).
26. Lindsley, D. L. & Zimm, G. G. *The Genome of* Drosophila melanogaster (Academic, San Diego, 1992).

ACKNOWLEDGEMENTS. We thank R. R. Ramey, L. Brown and the Sengwa Wildlife Research Institute for the Zimbabwe *D. melanogaster* sample, W. Eanes, G. Karpen, J. Lucchesi, P. Morcillo, K. O'Hare and L. Searles for clones and M. Nachman for comments. This research is supported by the NIH and NSF.

Macaque V1 neurons can signal 'illusory' contours

David H. Grosof*, Robert M. Shapley† & Michael J. Hawken

Center for Neural Science, New York University, 4 Washington Place, New York, New York 10003, USA

WE describe here a new view of primary visual cortex (V1) based on measurements of neural responses in V1 to patterns called 'illusory contours' (Fig. 1*a*, *b*). Detection of an object's boundary contours is a fundamental visual task. Boundary contours are defined by discontinuities not only in luminance and colour, but also in texture[1-3], disparity[4] and motion[5-7]. Two theoretical approaches can account for illusory contour perception. The cognitive approach emphasizes top-down processes[8,9]. An alternative emphasizes bottom-up processing. This latter view is supported by (1) stimulus constraints for illusory contour perception[10-14] and (2) the discovery by von der Heydt and Peterhans[15-17] of neurons in extrastriate visual area V2 (but not in V1) of macaque monkeys that respond to illusory contours. Using stimuli different from those used previously[15,16], we found illusory contour responses in about half the neurons studied in V1 of macaque monkeys. Therefore, there are neurons as early as V1 with the computational power to detect illusory contours and to help distinguish figure from ground.

We measured responses of 25 neurons in para-foveal V1 of anaesthetized monkeys to four types of patterns sharing the same mean luminance: sinusoidal luminance gratings (Fig. 1*c*); luminance edges (Fig. 1*d*); half-screen patches of sinusoidal luminance grating, in which the bar ends define an illusory contour oriented perpendicularly to the bars and located at the boundary between the grating patch and a blank portion of the stimulus screen at the same mean luminance (Fig. 1*e*); and two half-screen patches of grating abutting one another, in which the two patches are identical and in antiphase (Fig. 1*f*). Results obtained using the pattern in Fig. 1*f* resemble those shown in Fig. 1*e* (for example, the cell in Fig. 2*a* responded similarly to both).

Because the grating is periodic, it is natural to express its position relative to receptive field location as spatial phase: the starting spatial phase angle of the sinusoidal grating relative to the stimulus frame. For example, in Fig. 1*e* the spatial phase is 0 degrees. As phase varies, the position of grating bars with respect to fixed cell receptive fields varies so that, when the illusory contour is drifted, different values of black and white are swept across a receptive field.

We found responses to illusory contours drifted across a cell's receptive field in the preferred direction for a luminance edge (that is, when grating bars defining the illusory contours were perpendicular to the optimal orientation for an edge). A variety of responses to illusory contour patterns was observed. One type is illustrated in Fig. 2*a*: this direction-selective complex cell fired two bursts per period, one to each of the 'left-handed' and 'right-handed' boundaries of the central patch in Fig. 1*e*, *f*. Comparison of responses to luminance (Fig. 1*d*) and illusory contours (Fig. 1*e*, *f*) showed that the two bursts were synchronized to the passage of the illusory contour over the cell's receptive field. The cell in Fig. 2*a* signals the presence of a contour in its receptive field independent of contrast polarity: the stimulus when the illusory contour leaves the receptive field is opposite in sign to when it enters, but the cell's response is excitatory to both entry and exit. Our measure of this frequency-doubled response is the Fourier amplitude of the second harmonic (F2) of the post-stimulus time histogram. Another type of cell responded to just one of the two contours passing over the receptive field, illustrated by the response shown in Fig. 2*b*.

If a frequency-doubled response signifies the presence of illusory contours crossing a cell's receptive field, its magnitude should not depend on the precise position (spatial phase) of the illusory contour along the long axis of the receptive field. Figure 2 shows how response changed for two cells as spatial phase varied. The simple cell in Fig. 2*b* responded to the leading edge of the one-sided pattern from 1.75π to 0.25π radians, and to the trailing edge from 0.75π to 1.25π radians. This implies that the cell was responding simply to a bright bar-end entering the receptive field or to a dark bar-end leaving it. But the response of the cell shown in Fig. 2*a* was the same at all spatial phases, implying that it responded to contour and not simply to bar-endings.

An index of response-dependence on spatial phase was derived: the greatest (pairwise) difference in response, divided by the sum of the maximum and minimum response. Figure 3 shows the distribution of the index across complex cells (*a*) and simple cells (*b*). For most complex cells this index was less than 0.5; the indices of simple cells were distributed uniformly between 0-1. This implies that many cortical cells responded to extended contour, rather than to individual grating bar endings. Of the nine cells with phase modulation index of less than 50%, the median relative contrast sensitivity (grating threshold/illusory contour threshold) was 0.76 (range, 0.32-4.0). This means that the illusory contours were effective stimuli. We did not measure the length of the neurons' receptive fields, but spatial phase invariance implies nonlinear spatial summation along the grating-defined contour. A modification of the Spitzer-Hochstein[18] model for cortical complex cells may account for the illusory contour responses we observed. Misaligning that model's subunits in the axis parallel to the cell's preferred orientation, so that each subunit has a different centroid of sensitivity in the 'long axis' of the receptive field, will yield spatial phase insensitivity.

Responses to illusory contours defined by line gratings (as in Fig. 1*b*) were compared with those defined by sine gratings in eight neurons. The linewidth used was 1.2 arcmin, chosen to be like line-grating stimuli used in refs 15-17. The median ratio of peak responses to line/sine-defined illusory contours was 0.2. The linewidth in the line-defined illusory contour seems to be a

* Present address: Department of Ophthalmology and Visual Science, Washington University School of Medicine, St Louis, Missouri 63110, USA.
† To whom correspondence should be addressed.

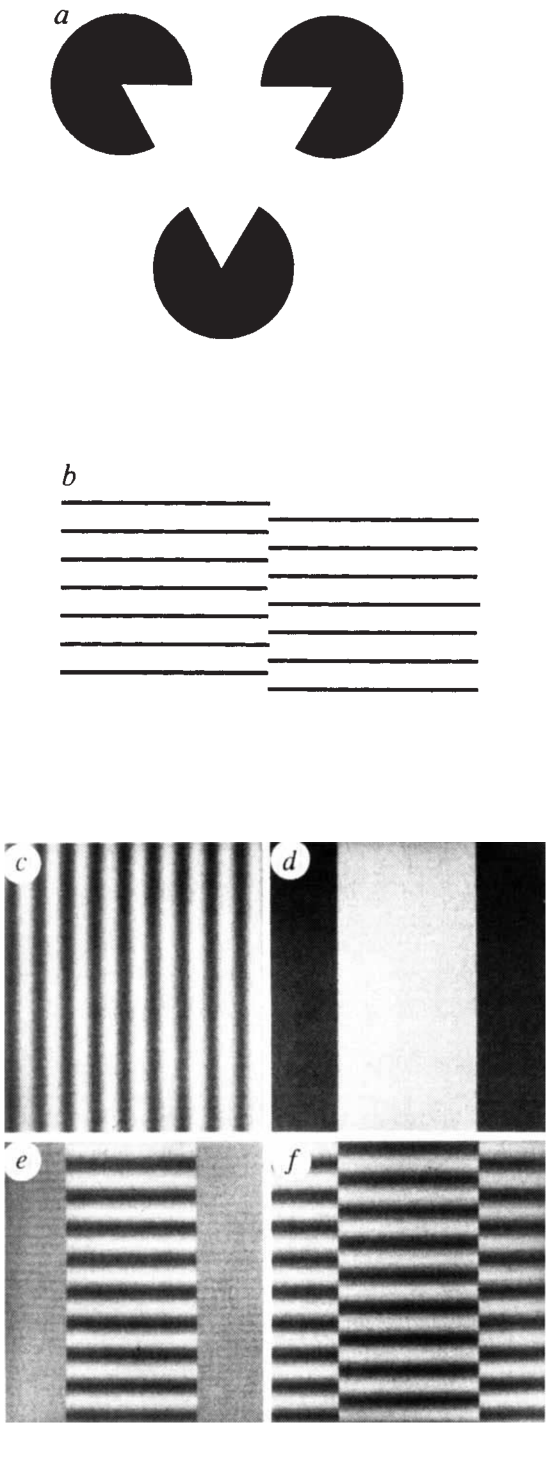

FIG. 1 Visual patterns. *a*, Kanizsa triangle. A triangle appears to occlude three circular disks. There is no change in luminance across the middle of each side of the triangle. *b*, Abutting line grating. A sharp edge appears where the two line gratings meet. *c*, Full-field sinusoidal grating. *d*, Simple luminance edges. Two edges of opposite contrast polarity divide the display into two rectangular patches. Motion direction is normal to the edges in *a* and *b*. *e*, 'One-sided' illusory contour pattern. A half-screen patch of grating defines two illusory contours, one on each side of the patch. The contours are perpendicular to the grating bars. The mean luminance of the blank portion of the screen is the same as that of the grating patch. *f*, 'Two-sided' illusory contour pattern. Two gratings differing only in their relative vertical position (spatial phase) define illusory contours at both abutments. The pattern motion was rigid horizontal translation in *c*–*f*; the direction was normal to the luminance edges in *c* and *d*, and normal to the vertical illusory contours in *e* and *f*.

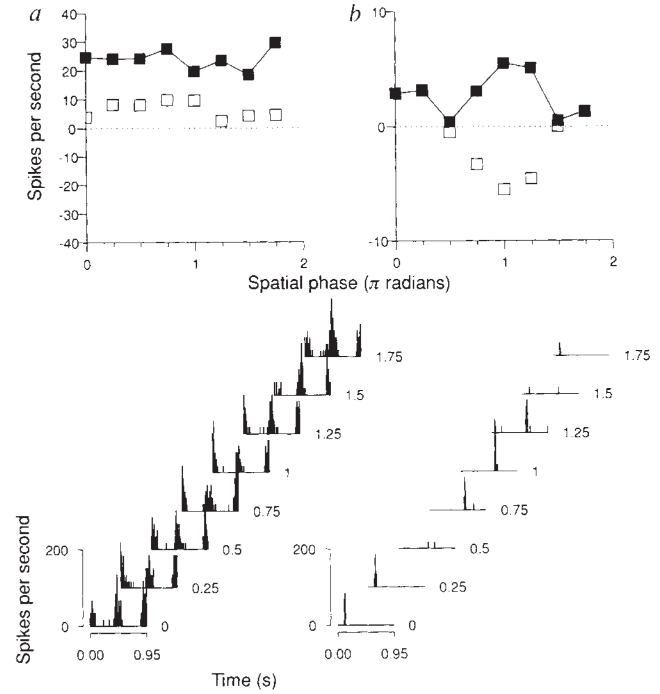

FIG. 2 Two types of striate response to illusory contour patterns of Fig. 1*e*. *a*, The lower series shows the peristimulus time histograms (PSTHs) of a layer-5, directionally selective, complex cell's responses to a one-sided (as in Fig. 1e) illusory contour pattern (1.3 cycles per degree grating, 80% contrast), drifted at 6 deg s^{-1} in the optimal edge direction and with the spatial phase (in π radians) written alongside each PSTH. Each pattern drifted to the edge of the screen, wrapped around, and returned to its starting position every 947 ms. Histogramming the spikes using a temporal period of 947 ms shows the cell responded to each of the two illusory contours passing over the receptive field in a period. The upper plot shows the amplitude of the first (F1, open squares) and second (F2, filled squares) harmonics of the PSTHs. The phase modulation index (see text) for this cell was 0.27. *b*, The lower plots show PSTHs of a simple cell in layer 5 to one-sided illusory contour patterns (0.7 cycles per degree grating, 80% contrast). The pattern is drifted at 6 deg s^{-1} in the optimal direction, at a series of spatial phases denoted to the right of each PSTH. As spatial phase is varied, the cell responds to one or the other of the illusory contours but never to both. The response virtually nulls at two spatial phases, spaced a half-cycle apart. The upper plot shows F1 and F2 varying with spatial phase. The sign of the F1 response is made negative to denote when temporal phase of the F1 harmonic changes sign. The near-sinusoidal dependence of F1 response on spatial phase is a signature of mechanisms with spatial summation linearity[23]. The phase modulation index is 0.80.

METHODS. Standard procedures were used in these acute recording experiments of cynomolgus monkeys (*Macaca fascicularis*; 2–6 kg). Anaesthesia was induced with ketamine (12–16 mg per kg body weight) intramuscularly and maintained with sufentanyl (6 μg kg^{-1} h^{-1}, intravenous). Local anaesthetic was applied to pressure points and incisions; electroencephalogram, electrocardiogram and blood pressure were monitored and anaesthesia supplemented as necessary with either acepromazine or sufentanyl. Extracellular action potentials were recorded from single neurons using glass-coated tungsten microelectrodes[24] with 5–15-μm exposed tips. Quantitative measurement was done with patterns displayed to the preferred eye on either a Tektronix 608 (P4 phosphor, 10 cm by 10 cm, 270-Hz frame rate, mean luminance 100 cd m^{-2}) CRT monitor or a colour Tektronix 690 (25.6 cm by 25.6 cm, 135 Hz frame rate, 67 cd m^{-2}) monitor. The scopes were controlled and gamma-corrected by a custom graphics instrument[25] and a PDP 11–83 computer. The cathode ray tubes were also calibrated with a Photo Research Model 703-PC spectroradiometer to make certain that there was no artefactual luminance difference between the blank and textured regions of the stimulus. Cells were classified using a modification[23] of the Enroth-Cugell and Robson null test. Histological processing and laminar assignment of neurons were as described in refs 26, 27.

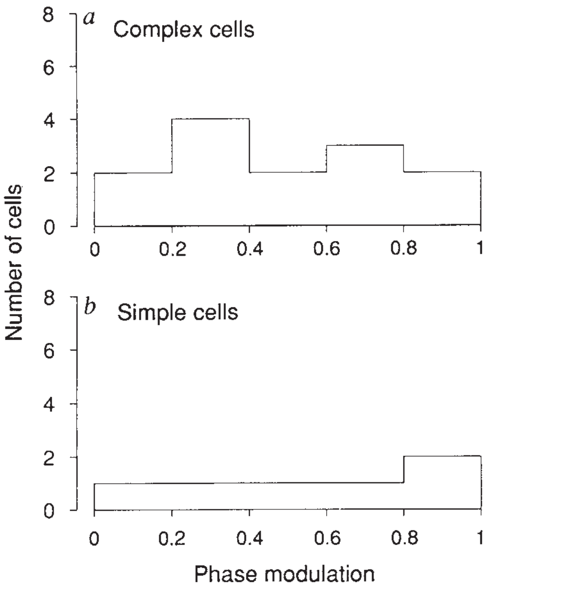

FIG. 3 Phase modulation index for: *a*, 13 complex and *b*, 6 simple cells. The index is the Michelson contrast of the array of F2s evoked by stimuli at different spatial phases: greatest (pairwise) difference in response divided by the sum of the maximum and minimum response. The index indicates whether a response to the illusory contour depends on the precise position of the grating patch perpendicular to the illusory contour: an index of one means the cell has a null spatial phase and zero means the response is invariant to changes in spatial phase. The stimulus contrast of the gratings used to induce the contours was 60–80%.

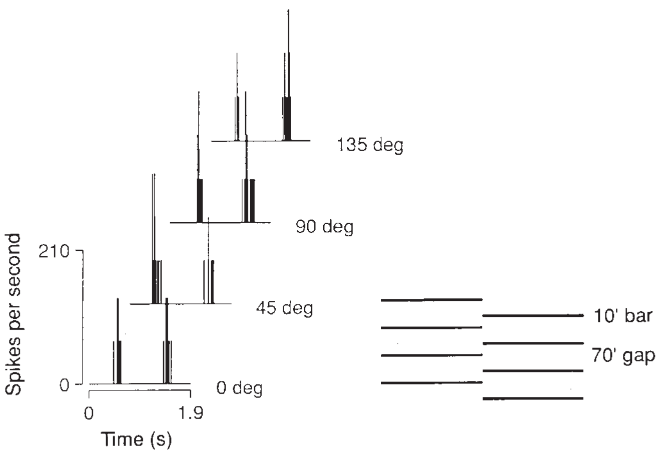

FIG. 4 Response of a V1 complex cell to abutting line gratings. The stimulus is depicted on the right side of the figure; each grating had a period of 80 arcmin, with a linewidth of 10 arcmin, and a gap between lines of 70 min. The gratings were always offset from each other by half a cycle, irrespective of spatial phase, creating an illusory contour at the line of abutment, as in Fig. 1*b*. The bars' luminance was ~0.5 cd m^{-2} against a background of 100 cd m^{-2}. The left side of the figure depicts the responses of the neuron at four different spatial phases, with the same format as in Fig. 2. The pattern was drifted continuously, with 'wraparound' and the drift speed was 2.3 deg s^{-1} (~0.5 Hz).

critical variable. We were able to measure phase-insensitive illusory contour responses in a V1 neuron with line gratings in which the lines were 10 arcmin wide (Fig. 4); however, this same neuron did not respond to line gratings with lines 1 arcmin wide.

The ability of illusory contour-responsive neurons to ignore contrast polarity and boundary type suggests that they convey information about the location and orientation of object borders salient for segmentation[19–21]. These results indicate that V1 neurons perform sophisticated image processing and that V1 is an image-processing area, rather than simply a spatially transformed replication of the retina. Our results and conclusions are consistent with a recent report[22] that motion-defined contours also produce responses in V1 cortex. □

Received 7 April; accepted 16 July 1993.

1. Beck, *J. Biol. Cybern.* **48,** 125–130 (1983).
2. Julesz, B. *IRE Trans. Inf. Theory.* *IT*-8, 84–92 (1962).
3. Julesz, B. *Nature* **290,** 91–97 (1981).
4. Julesz, B. *Foundations of Cyclopean Perception* (Univ. Chicago Press, Chicago, 1971).
5. Nakayama, K. & Tyler, C. W. *Vis. Res.* **21,** 427–433 (1981).
6. Nakayama, K., Silverman, G. H., MacLeod, D. I. A. & Mulligan, J. *Perception* **14,** 225–238 (1985).
7. van Doorn, A. J. & Koenderink, J. J. *Expl Brain Res.* **45,** 179–195 (1982).
8. Gregory, R. L. *Nature* **238,** 51–52 (1972).
9. Rock, I. & Anson, R. *Perception* **8,** 665–681 (1979).
10. Smith, A. & Over, R. *Perception* **6,** 441–447 (1977).
11. Smith, A. & Over, R. *Perc. Psychophys.* **25,** 95–98 (1979).
12. Paradiso, M. A., Shimojo, S. & Nakayama, K. *Vis. Res.* **29,** 1205–1213 (1989).
13. Gregory, R. L. *Perception* **6,** 113 119 (1977).
14. Takahashi, S., Kaihara, T., Takemoto, A., Ido, K. & Ejima, Y. *Vis. Res.* **32,** 1709–1718 (1992).
15. von der Heydt, R., Peterhans, E. & Baumgartner, G. *Science* **224,** 1260–1262 (1984).
16. von der Heydt, R. & Peterhans, E. *J. Neurosci.* **9,** 1731–1748 (1989).
17. Peterhans, E. & von der Heydt, R. *J. Neurosci.* **9,** 1749–1763 (1989).
18. Spitzer, H. & Hochstein, S. *J. Neurophysiol.* **53,** 1266–1286 (1985).
19. Shapley, R. & Gordon, J. *Perc. Psychophys.* **37,** 84–88 (1985).
20. Shapley, R. & Gordon, J. in *The Perception of Illusory Contours* (eds Petry, S. & Meyer, G. E.) 109–115 (Springer, New York, 1988).
21. Grossberg, S. & Mingolla, E. *Psychol. Rev.* **92,** 173–211 (1985).
22. Lamme, V. A. F., van Dijk, B. W. & Spekreijse, H. *Nature* **363,** 541–543 (1993).
23. Hochstein, S. & Shapley, R. M. *J. Physiol., Lond.* **262,** 237–264 (1976).
24. Merrill, E. G. & Ainsworth, A. *Med. Biol. Engng* **10,** 662–672 (1972).
25. Milkman, N. *et al. Behav. Res. Meth. Instrum.* **12,** 283–292 (1980).
26. Wong-Riley, M. *Brain. Res.* **171,** 11–28 (1979).
27. Hawken, M. J., Parker, A. J. & Lund, J. S. *J. Neurosci.* **8,** 3541–3548 (1988).

ACKNOWLEDGEMENTS. We thank J. Gordon and F. Mechier for help with the experiments, N. Milkman for hardware and software modifications, and J. Beusmans, K. Gegenfurtner and D. Kiper for comments on the manuscript. This work was supported by grants from the US National Eye Institute (R.S. and M.H.) and an NRSA postdoctoral fellowship (D.G.).

Protein tyrosine kinase p56^{lck} controls allelic exclusion of T-cell receptor β-chain genes

Steven J. Anderson, Steven D. Levin & Roger M. Perlmutter*

Howard Hughes Medical Institute and the Departments of Immunology, Biochemistry and Medicine (Medical Genetics), University of Washington School of Medicine SL-15, Seattle, Washington 98195, USA

DURING T-cell development, site-specific DNA rearrangements mediating assembly of β- and α-chain genes of the T-cell receptor (TCR) are developmentally ordered[1,2]. In particular, assembly and expression of a complete β-chain gene blocks further rearrangements at the β-locus (a process referred to as allelic exclusion)[3] and drives the generation and expansion of $CD4^+8^+$ cells[4,5]. Although the mechanism used by TCRβ chains to deliver such signals is unknown, studies in transgenic animals have suggested that the lymphocyte-specific protein tyrosine kinase p56^{lck} may impinge on a similar signalling pathway[6]. The hypothesis that TCRβ chains deliver intracellular signals via p56^{lck} makes an explicit prediction: that interference with p56^{lck} function will mitigate the effects of a simultaneously expressed TCRβ chain. Here we confirm this prediction through examination of allelic exclusion in mice expressing both a functional TCRβ chain transgene and a catalytically inactive form of p56^{lck}.

p56^{lck} participates in TCR-derived signalling[7] in part through a physical association with the coreceptors CD4 and CD8[8,9]. In addition, a critical role for this kinase during early thymocyte

* To whom correspondence should be addressed.